

Common-Offset and Common-Offset-Vector Migration of 3D Wide Azimuth Land Data: A Comparison of Two Approaches

Mike Perz*

Divestco Inc, Calgary, AB
mike.perz@divestco.com

and

Ye Zheng

Divestco Inc, Calgary, AB, Canada

Summary

Common-offset (CO) 3D Kirchhoff prestack time migration is routinely used in processing unstructured land data, yet the algorithm violates sampling theory by ignoring azimuth distribution. Moreover, orthogonal acquisition geometries do not admit a “natural” binning of the input data during the formation of CO volumes. In an effort to understand why the algorithm works well in spite of these theoretical blemishes, we study a synthetic data set simulating a stratigraphic channel play. We compare the CO migrated image to that obtained using common-offset-vector (COV) migration, the latter algorithm providing better localization in the azimuth domain (Cary, 1999). Preliminary tests show that an industrial-strength implementation of CO migration gives an excellent stacked image, thereby corroborating our real world observation that CO migration often works very well. However, a more bare-bones version of CO migration shows more sampling artifacts relative to the COV algorithm, implying that the theoretical violations inherent in CO migration are indeed lurking in the background. Finally, we show that offset-indexed gathers produced by COV migration show poor resolution in the offset domain relative to those produced by CO migration.

Introduction

3D common-offset Kirchhoff prestack time migration has achieved “workhorse” status in the imaging of stratigraphic land data sets, especially for amplitude-versus-offset (AVO) processing. In spite of its popularity, the algorithm violates the rules of sampling theory by mixing widely-varying source-receiver azimuths. It is well-known that irregular variation in azimuth sampling can give rise to artifacts in the migrated image via imperfect operator cancellation (e.g., Abma et al., 2007, Gardner and Canning, 1994). Moreover, it is difficult to form single-fold CO input volumes for typical acquisition geometries, giving rise to another potential source of artifacts. In spite of these two issues, experience has shown that the algorithm works well in a great number of cases, suggesting that neither issue represents a serious limitation all of the time. Still, in many cases we *do* observe an unacceptable level of artifact, and we are driven to explore the question of whether there is something we can do to improve the result.

Recently, Margrave and Cooper (2008) generated a 3D prestack synthetic dataset which simulates acquisition across a stratigraphic channel play. In this paper we use this data set to carefully study the performance of CO migration and to compare it to COV migration, an algorithm that offers better localization in the azimuth domain and also permits a more regular data binning.

Theory

We begin by considering an idealized acquisition scenario in which all sources and receivers share precisely the same offset and azimuth, and a single input trace exists at every cmp location. The Kirchhoff migration of this single common offset and azimuth (COA) volume entails performing a weighted summation of the input data over the familiar diffraction traveltime surface, where the summation proceeds across the midpoint-x and midpoint-y (inline and crossline) midpoint coordinates. If the inline and crossline sampling is sufficiently dense (and certain details of implementation such as operator antialiasing are carefully treated), this discrete summation will give a good approximation to the underlying continuous-variable spatial integral, an integral which has been carefully studied by workers in the field of true amplitude migration. In particular, if we use migration weights prescribed by Bleistein (2001), the output image gives an estimate of angle dependent reflectivity consistent with the acoustic wave equation (under certain simplifying assumptions). It follows that this COA discrete summation enjoys a certain amount of theoretical underpinning, and thus it will serve as a useful launching pad into the real world situation of sparse and/or irregular acquisition.

For sparsely sampled wide-azimuth land data, it's impossible to achieve perfect localization in either offset or azimuth domain, so we must perform some binning of the input data prior to implementing a summation such as the one described above. One good strategy would be to choose offset and azimuth bin widths so that the resulting unmigrated COA volumes provide input data support at each cmp location (i.e., a single input trace exists at each cmp location). Unfortunately, for typical land acquisition patterns, it is impossible to achieve a uniform cmp fold within such COA volumes. Instead the fold tends to fluctuate from cmp to cmp and gaps may exist in the coverage. One approach to reducing artifacts brought on by this irregular fold distribution is to "pre-normalize" each input data sample by $1/N$ prior to implementing the summation, where N is the fold. This "normalized summation" approach may be described by:

$$I_{COAij}^{p,k} = \sum_l \sum_m W_{ijklm} D_{lm}, \quad D_{lm} = \frac{1}{N(l,m)} \sum_{n=1}^{N(l,m)} d_{lm,n}^{\tau(i,j,k,l,m,n;p,v)} \quad (1)$$

where $I_{COAij}^{p,k}$ is the output migrated image at the k^{th} time sample, i^{th} inline and j^{th} crossline (i.e., $cmp=(l,j)$) associated with the p^{th} COA volume, W_{ijklm} are the migration weights, $N(l,m)$ is the offset and azimuth limited fold at $cmp(l,m)$, and $d_{lm,n}^{\tau(i,j,k,l,m,n;p,v)}$ is the n^{th} input data trace at $cmp(l,m)$ which we choose to evaluate at $time=\tau(i,j,k,l,m,n;p,v)$ (i.e., the sum of the traveltimes from source-to-image-point and receiver-to-image-point, which also depends on velocity, v). This normalized summation can be combined with the above data binning strategy (i.e., choose bin sizes which give input data support at every cmp) in a practical implementation of COV migration since the latter algorithm is very similar to COA migration. In fact, COV migration gives an *implicit* localization in azimuth and offset via an *explicit* localization of inline and crossline offsets during the formation of input COV volumes. It turns out that extension of this same input-data-binning-plus-normalized-summation process to CO migration also works quite well in practice (Zheng et al., 2001).

The “recipe” for COV binning (i.e., how to choose inline and crossline bin widths to achieve optimal input data support) is cast in Cartesian coordinates, and for perfectly regular orthogonal acquisition each COV volume gives 1-fold coverage at each cmp location. By contrast, the CO binning recipe is cast in polar coordinates, and this precludes such a “natural” binning of the data. Figures 1a and 1b show the fold plots for representative CO and COV input volumes, respectively, for the case of regular orthogonal acquisition. Note that the CO fold fluctuates considerably across cmp’s (and that some holes exist in the coverage) despite our best efforts at binning, while the COV fold shows the expected homogeneous distribution away from the edges (the fold is 2 everywhere, not 1, because we have invoked source-receiver reciprocity in our binning.)

Synthetic Data Testing

The synthetic channel data set was generated using a shot domain acoustic modeling algorithm. Details are provided in Cooper et al. (2008) and Margrave and Cooper (2008). The earth model contains a synthetic channel reflector composed of a spatially invariant “regional” reflector atop which a sinuous low impedance channel and several point diffractors have been superimposed. Figure 2b shows the stacked image at channel level obtained using an industrial strength CO migration algorithm (the stack is created by summation of each individual CO volume). The algorithmic is an implementation of equation (1) that is augmented by several empirically-rooted “cosmetic” enhancements. This image gives a good delineation of the channel boundaries and point diffractors. Because the introduction of these cosmetic tricks precludes an apples-to-apples comparison with COV migration, we generated another “barebones” CO migration (same input CO bin sizes), this time via a “verbatim” implementation of equation (1) (Figure 2a). Figure 2c shows the COV migration result, where again a “verbatim” implementation of equation (1) has been used. Since we used identical (azimuth-independent) migration weights and post-migration mutes for both “barebones CO” and COV migrations, the only difference between the two migration algorithms (aside from the obvious fact that the input data volumes are binned differently) is the choice of normalizing factor $N(l,m)$ in equation (1). Comparing Figures 2a and 2c, it is clear that the CO migration shows more artifacts. In fact, the COV migration image is comparable in quality to the industrial strength CO migration in Figure 2b, though the former algorithm lacks the benefit of any cosmetic tricks.

Although the COV migration seems to generate less acquisition-based migration artifacts, it carries a significant limitation. Specifically, the migrated COV volumes show poor localization in the polar (i.e., absolute) offset domain. Figure 3a shows a migrated gather indexed by offset after CO migration. Figure 3b shows the corresponding gather after COV migration. Inspection of the bottom annotation, which shows the nominal polar offset associated with each CO/COV volume, reveals the poor offset localization in the COV result (it should be noted that the channel reflector is so shallow that many of the offsets fail to survive the post-migration “NMO stretch” mute).

Conclusions

Synthetic experiments show that an industrial strength CO migration gives a good image, but a careful comparison between a barebones CO implementation and the corresponding COV migration shows that the CO migraton is actually producing more artifacts. One potential drawback of COV migration is that its migrated gathers lack localization in the polar offset domain, a fact which might compromise downstream processes like AVO inversion and/or migration velocity analysis. Additional work is required to ascertain whether the CO migration artifacts stem from fold fluctuations within each input CO volume (in practice with irregular sampling, this effect is not always as pronounced) or from imperfect migration operator cancellation due to trace-to-trace

variations in azimuth. Real data examples and additional synthetic results will be shown in the oral presentation.

Acknowledgements

We thank Joanna Cooper and Dr. Gary Margrave for use of their synthetic data set, Dr.'s Peter Cary and Zhengsheng Yao for helpful discussions, and Divestco Inc. for allowing us to present this work.

References

- Abma, R., Kelley, C., and Kaldy, J., 2007, Sources and treatments of migration-introduced artifacts and noise: 77th Ann. Int. Mtg., SEG, Exp. Abs., 2349-2353.
- Bleistein, N., Cohen, J.K., and Stockwell, J.W., 2001, Mathematics of multidimensional seismic imaging, migration and inversion: Springer Press.560 pp.
- Cary, P.W., 1999, Common-offset-vector gathers: an alternative to cross-spreads for wide-azimuth 3-D surveys: 69th Ann. Int. Mtg., SEG, Exp. Abs., 1496-1499.
- Cooper, J.K., Margrave, G.F., and Lawton, D.C., 2008, Simulations of seismic acquisition footprint: 2008 CSEG Ann. Mtg: submitted.
- Gardner, G. H. F., and A. Canning, 1994, Effects of irregular sampling on 3-D prestack migration: 64th Annual International Meeting, SEG, Expanded Abstracts , 1553-1556
- Margrave, G.F., and Cooper, J.K., 2008, Seismic modeling in 3D for migration testing: 2008 CSEG Ann. Mtg: submitted.
- Zheng, Y., S. Gray, S. Cheadle, and P. Anderson, 2001, Factors affecting AVO analysis of prestack migrated gathers: 71st Ann. Int. Mtg., SEG, Exp Abs. , 989-992

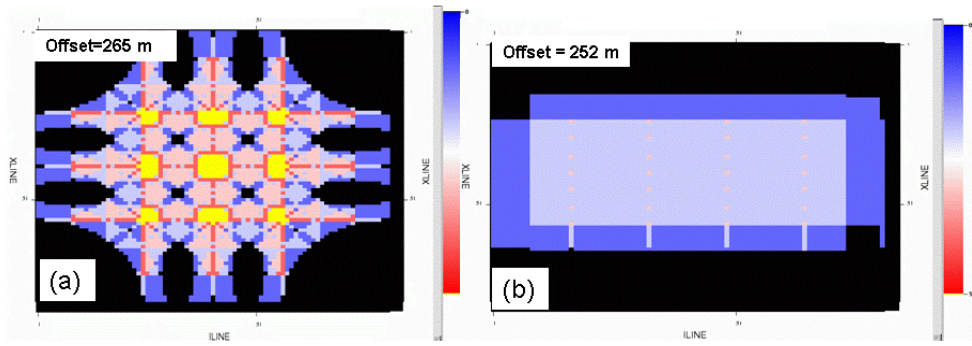


Figure 1: CMP-fold displays from Cooper et al. synthetic data set. (a) CO volume with centre offset=265 m and offset bin full width =50 m; (b) COV volume with centre inline offset=80 m, centre crossline offset=240 m, inline offset bin full width= crossline offset bin full width=160 m. Nominal polar offset is $\sqrt{80^2+240^2}=252$ m.

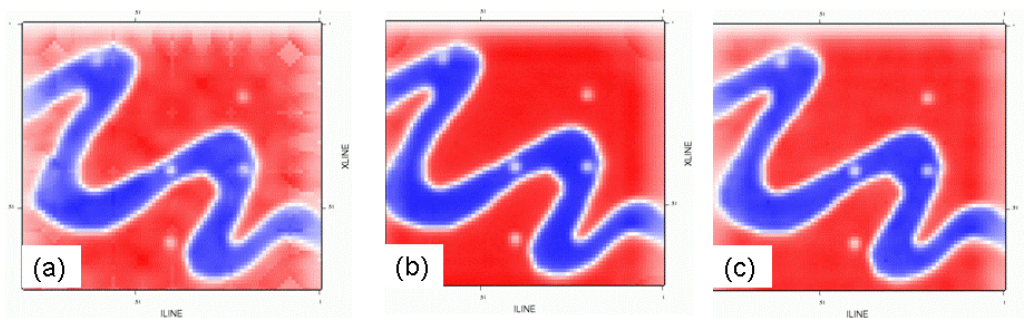


Figure 2: Migrated time slices at channel level. (a) "barebones" CO migration; (b) "industrial strength" CO migration; (c) COV migration

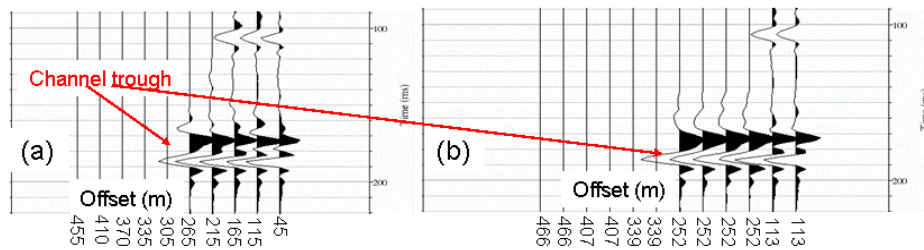


Figure 3: Migrated gathers indexed by polar offset at a CMP located directly beneath the channel. (a) CO migration; (b) COV migration.